Editor's Choice paper

Full kinetic description of 1-octene hydroformylation in a supercritical medium

Ard C.J. Koeken [a],[*], Leo J.P. van den Broeke [a],[1], Berth-Jan Deelman [b],[2], Jos T.F. Keurentjes [a]

[a] *Process Development Group, Eindhoven University of Technology, P.O. Box 513, 5600 MB Eindhoven, The Netherlands*
[b] *Arkema Vlissingen B. V., P.O. Box 70, 4380 AB Vlissingen, The Netherlands*

ARTICLE INFO

ABSTRACT

The kinetics of the hydroformylation of 1-octene in a supercritical carbon dioxide medium, catalyzed by a tris(3,5-bis[trifluoromethyl]phenyl)phosphine-modified rhodium catalyst, have been investigated. The influence of the concentration of carbon dioxide, reactants, catalyst precursors, and the reaction temperature has been determined. A kinetic model was developed, which describes the concentration-time profiles of the reactants, the linear and branched aldehydes, and the internal alkenes. Using the kinetic model activation energies for hydroformylation of 1-octene to nonanal and 2-methyloctanal were determined. Throughout the concentration ranges studied an approximate first order dependence of the hydroformylation rate on the hydrogen and catalyst concentration was found which indicated that oxidative addition of hydrogen was the rate limiting step. The increase in reaction rate and regioselectivity with an increase in ligand concentration is a striking feature of the catalyst investigated here. At higher concentrations the reaction rate was found to have a strong negative order dependence on the carbon monoxide concentration. The reaction rate had a positive order in 1-octene at a concentration lower than $0.5 \, \mathrm{mol} \, \mathrm{L}^{-1}$ while saturation kinetics were observed at a higher concentration. The results were explained by invoking the contribution of both monophosphine and diphosphine rhodium species to the hydroformylation catalysis.

© 2011 Elsevier B.V. All rights reserved.

1. Introduction

Hydroformylation of alkenes using homogeneous catalysts is applied on a commercial scale to make aldehydes that serve as starting materials for the production of detergents, plasticizers, and solvents [1–4]. Consequently, controlling the kinetics of hydroformylation reactions is a field of high current interest [4]. The applied catalysts are complexes of rhodium or cobalt, commonly with phosphines or phosphites as modifying ligands. In order to reuse the catalyst, separation steps like distillation or extraction are required, which could, in principle, have a detrimental effect on catalyst activity and selectivity. The Ruhrchemie/Rhône-Poulenc (RCH/RP) hydroformylation process is a well-known example where, by means of an aqueous phase which preferentially dissolves the catalyst, the reaction and the separation step of the homogeneous rhodium catalyst are integrated [5]. However, this approach is limited to the hydroformylation of short-chain alkenes,

because long-chain alkenes are too sparingly soluble in water to obtain acceptable space-time yields [6].

Supercritical fluids have received considerable attention as alternative reaction media for the hydroformylation of long-chain alkenes such as 1-octene [7]. Supercritical carbon dioxide (scCO$_2$) is of particular interest since it has accessible critical properties, is nonflammable, is easily separated from the reaction product by depressurization, and has a low toxicity. Furthermore, a single-phase reaction system can be created with a high diffusivity of the dissolved species and a high solubility of permanent gases like carbon monoxide and hydrogen [8].

One of the restrictions of applying scCO$_2$ as a solvent is the limited solubility of common homogeneous catalysts in this medium. For hydroformylation, carbonylation and hydrogenation catalysts this drawback has been primarily overcome by modifying ligands with certain functional groups [9–31] or by using phosphines of low molecular weight [32,33]. Recently, it was demonstrated that even rhodium catalysts modified with the well-known triphenylphosphine or triphenyl phosphite ligand were applicable with high efficiency in CO$_2$-rich supercritical medium when high densities were applied [34]. An alternative approach to using a single phase supercritical medium is the application of a CO$_2$ expanded organic solvent. CO$_2$ expanded solvents appear to allow for improved hydroformylation selectivity in some cases [35,36]. Attaching perfluoroalkyl groups on the ligands of the catalyst appears to be the most effective means to ensure a sufficient catalyst solubility in a

---

* Corresponding author. Present address: Inorganic Chemistry and Catalysis, Utrecht University, Universiteitsweg 99, 3584 CG Utrecht, The Netherlands. Tel.: +31 622736392.

E-mail addresses: a.c.j.koeken@uu.nl, ardkoeken@hotmail.com (A.C.J. Koeken), berth-jan.deelman@arkema.com (B.-J. Deelman).
[1] Present address: TNO Science and Industry, Separation Technology, Schoemakerstraat 97, P.O. Box 6012, 2600 JA Delft, The Netherlands.
[2] Fax: +31 113 612984.
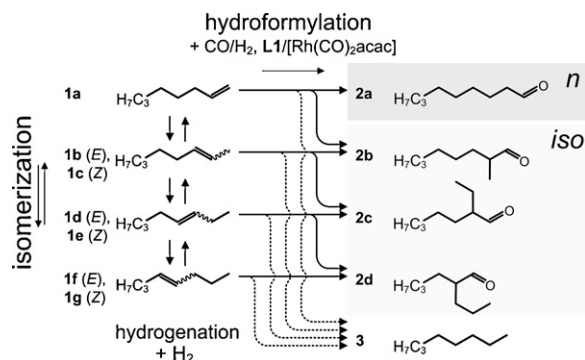
Scheme 1. Reaction scheme for the hydroformylation of 1-octene (**1a**), with the two main products nonanal (**2a**) and 2-methyloctanal (**2b**). The side products are (*E*,*Z*)-2-octene (**1b**, **1c**), (*E*,*Z*)-3-octene (**1d**, **1e**), (*E*,*Z*)-4-octene (**1f**, **1g**), 2-ethylheptanal (**2c**), 2-propylhexanal (**2d**), and *n*-octane (**3**).

CO_2-rich reaction medium. The 'tunability' of the solvent properties of $scCO_2$ by relatively small changes in temperature and pressure allows the precipitation and reuse of the perfluoroalkyl-substituted catalysts [9,10]. Furthermore, catalyst activity and selectivity can be enhanced by attachment of perfluoroalkyl groups on phosphine ligands used in hydroformylation [37].

Although there is significant current interest in using $scCO_2$ as solvent for hydroformylation, detailed kinetic studies in single phase supercritical media are scarce. There is a study by Erkey and co-workers which deals with tris(3,5-bis[trifluoromethyl]phenyl)phosphine (**L1**) modified Rh [38]. In that study relatively low temperatures (40–50 °C) and a relatively low and constant initial pressure were used. Turnover frequencies (TOF) in the range of 1000–2000 $mol_{aldehyde} \, mol_{Rh}^{-1} \, h^{-1}$ and a negligible isomerization of 1-alkene were observed. The kinetic model developed in that study did not include the regioselectivity of the reaction nor did it include isomerization of the 1-alkene.

Using the same system as studied by Davis and Erkey [38] we recently found for $scCO_2$ that application of a higher temperature (i.e. 70 °C instead of 50 °C) and a higher pressure (i.e. 40–50 MPa instead of 28 MPa) resulted in considerably higher, and therefore industrially more attractive TOF values [13,14]. Here, an extensive description of the reaction kinetics of 1-octene (**1a**) hydroformylation covering a wider range of conditions is presented, which describes the overall reaction rate as well as the chemo- and regioselectivity as a function of the concentration of reactants and catalyst precursors (Scheme 1). The relation between the observed kinetics and the catalytic cycle is discussed and the results are compared to other kinetic studies of rhodium-catalyzed hydroformylation of linear 1-alkenes.

2. Experimental

2.1. Materials

Carbon dioxide, carbon monoxide, and hydrogen, grade 5.0, 4.7, and 5.0, respectively, were obtained from Hoekloos (The Netherlands). Prior to use CO_2 was passed over a Messer Oxisorb filter to remove oxygen and moisture. 1-Octene, **1a**, obtained from Aldrich, was passed over activated alumina, dried with pre-treated molsieves 3A (Aldrich, 4–8 mesh), and stored under argon. The rhodium precursor, rhodium(I) dicarbonyl acetylacetonate, [Rh(CO)$_2$acac], was obtained in the form of dark green crystals from Fluka. Ligand **L1**, tris(3,5-bis[trifluoromethyl]phenyl)phosphine, is a white to light yellow solid and was supplied by Arkema (Vlissingen, The Netherlands). All catalyst precursors were stored under argon. The solvent toluene (Merck, analytical grade), the internal standard *n*-decane (Aldrich, >99% purity) and the substances

involved in the reaction, *n*-octane (Aldrich, >99%), 2-octene (ABCR, mixture of *E* and *Z*, 98%), and nonanal (Fluka, >95%) used for the GC-analysis were used as received.

2.2. Hydroformylation in carbon dioxide

The details of the high pressure batch reactor setup are described in Ref. [39]. A typical hydroformylation experiment was started by charging the desired amounts of [Rh(CO)$_2$acac] and the phosphine ligand into the empty reactor and subsequently closing the reactor. Fig. 1 shows an example of typical conditions in terms of temperature (a) and pressure (b) during an experiment.

The reactor volume was carefully filled with argon and subsequently evacuated for three times. Next, the stirring was switched on with a stirring rate of 700 rpm and the desired amounts of carbon monoxide and hydrogen gas were charged to the reactor at room temperature (see Fig. 1b: at $t = -1.5$ h up to about 7.4 MPa in this case). The reactor content was heated to a temperature of 50 °C (Fig. 1a: at $t = -1.4$ h), and consecutively CO_2 was charged into the reactor at a constant flow typically up to a total pressure such that about 14.5 mol L^{-1} CO_2 was present (Fig. 1b: at $t = -1.2$ h). In the case when 1 mol L^{-1} of CO, 1 mol L^{-1} of H$_2$, and 14.5 mol L^{-1} of CO_2 was applied this corresponded to about 26 MPa total pressure at 50 °C. When the CO and H$_2$ concentration were varied, the total reactor pressure required to achieve a CO_2 concentration of 14.5 mol L^{-1} at 50 °C was estimated using the Peng–Robinson equation of state and the binary interaction coefficients as previously reported in Ref. [39]. A period of at least 0.5 h at reaction temperature was taken for the *in situ* formation of the active catalyst complexes from the [Rh(CO)$_2$acac] and **L1** (Fig. 1: $t = -0.5–0$ h). The reaction was started by the addition of **1a**, which was done by opening the valve between the pump and the reactor. Fast pressure equalization occurred and consecutively the desired volume
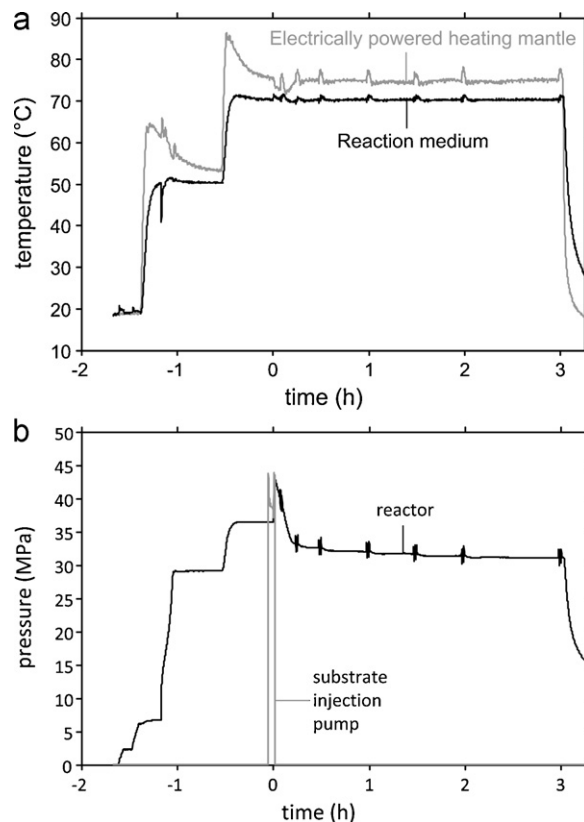
Fig. 1. (a) Typical temperature – time history during a hydroformylation experiment; (b) corresponding pressure – time history.

of **1a** was pumped into the reactor, which generally did not take more than 30 s. While pumping **1a** into the reactor, the medium temperature increased 1–3 °C as a result of a fast pressure increase and the start of the exothermic reaction (Fig. 1: $t \approx 0$ h). The temperature stabilized within 15 min. During the remainder of reaction the reactor temperature was maintained within a deviation of less than 1 °C from the desired temperature.

Samples were withdrawn from the high pressure mixture at regular intervals into a calibrated volume of 0.182 mL. The 'spikes' in pressure and temperature at regular time intervals are a result of sampling. At typical reaction conditions the change in pressure as a result of taking a sample was in between 0.1 and 0.2 MPa. The content of the sample volume was carefully bubbled through a vial with a solution of n-decane in toluene and afterwards rinsed with additional toluene solution to collect residual **1a** and its reaction products quantitatively. Subsequently, the sample volume was dried by alternately applying an argon flow and vacuum. The time for taking a sample and preparing for a next one was in the order of 10 min. Generally, a minimum reaction time of 3 h was observed, after which the reaction mixture was rapidly cooled, the gases were vented and the remaining liquids consisting of reaction products and catalyst were collected.

To ensure that the reactor was cleaned properly, blank reaction runs were performed regularly. The concentration of catalyst precursors were chosen such that catalytic complexes would dissolve completely for the conditions applied here.

2.3. Analysis and calibration

The samples were analyzed off-line using a Fisons Instruments GC-FID equipped with a Restek Rtx-5 column (fused silica, length 30 m, internal diameter 0.53 mm) with helium as the carrier gas. Calibration was done for **1a**, E-2-octene and Z-2-octene (**1b** and **1c**), n-octane (**3**) and nonanal (**2a**), the response factors for the other octene and aldehyde isomers were taken to be equal to those of **1a** and **2a**, respectively.

2.4. Reaction parameters

To obtain normalized concentration profiles for **1a** and its reaction products, each concentration obtained by GC analysis, $C_{GC,i}$, was divided by the sum of all obtained concentrations and multiplied by the concentration based on the total amount of **1a**, n_{1a} in mol, injected and the reactor volume, $V_{reactor}$ in L:

$$C_i = \frac{C_{GC,i}}{\sum_i C_{GC,i}} \times \frac{n_{1a}}{V_{reactor}} \qquad (1)$$

for i = **1a–1g**, **2a–2d** and **3**.

The outcome of the hydroformylation was expressed in one of the following parameters. The definitions used were based on Westerterp et al. [40]. The conversion, X, was given by:

$$X = \frac{C_{1a,0} - C_{1a}}{C_{1a,0}} \times 100\% \qquad (2)$$

The subscript 0 indicates the normalized concentration at $t = 0$ h.

The overall selectivity, S_i, towards a product i was defined as:

$$S_i = \frac{C_i}{C_{1a,0} - C_{1a}} \times 100\% \qquad (3)$$

where C_i is the normalized concentration of a product i, with i = **1b–1g**, **2a–2d** or **3**.

The overall yield, Y_i, for a product i was then:

$$Y_i = \frac{C_i}{C_{1a,0}} \times 100\% \qquad (4)$$

The initial overall rate of reaction R_0 (units mol s^{-1}), were estimated by multiplying the initial amount of **1a** in mol, $n_{1a,0}$, with the slope

of a line fitted through the conversion or yield data points up to a conversion where there was a linear trend (typically up to a conversion of 60%). A distinction is made between the linear aldehyde product, **2a**, and total amount of aldehydes, **2a–2d**, abbreviated as '**ald**'. So, $R_{1a,0}$, $R_{ald,0}$, $R_{2a,0}$, and $R_{1b-g,0}$ are the rate of conversion of **1a**, the rate of formation of aldehydes, the rate of formation of **2a**, the rate of isomerization of **1a**, respectively.

The TOF based on the formation rate of aldehydes was calculated as follows:

$$TOF_{ald} = \frac{R_{ald,0}}{n_{Rh}} \times \frac{3600\,s}{1\,h} \qquad (5)$$

where n_{Rh} is the amount of Rh in mol. The (cumulative) n:iso ratio was obtained by dividing the concentration of linear aldehyde product by the sum of the concentrations of the branched aldehyde products:

$$n:iso = \frac{C_{2a}}{C_{2b} + C_{2c} + C_{2d}} \qquad (6)$$

The initial differential n:iso ratio, $n:iso_0$, was estimated with the following equation:

$$n:iso_0 = \frac{R_{2a,0}}{R_{ald,0} - R_{2a,0}} \qquad (7)$$

The initial differential selectivity for **2a** was calculated with the following equation:

$$S_{2a,0} = \frac{R_{2a,0}}{R_{1a,0}} \qquad (8)$$

2.5. Kinetic model

The concentration profiles of carbon monoxide and hydrogen were determined from their initial concentration and the stoichiometry of the reactions. The reaction network used for the kinetic model (Scheme 2) was based on the reactions described in Scheme 1. The main internal octene isomers are E-2-octene (**1b**) and Z-2-octene (**1c**). The other octene isomers (**1d–1g**) were observed to some extent in the GC analysis but in very small amounts. Therefore, isomers **1b**, **1c** and the other octene isomers were lumped together as **1bc**. Similarly, the aldehyde isomers **2b**, **2c**, and **2d** were lumped together as **2bcd**.

Besides hydroformylation, isomerization of **1a** and hydrogenation of **1a** and its isomers are taken into account. The model allows for a description of the n:iso ratio, because the formation of linear (**2a**) and branched aldehydes (**2b**, **2c**, **2d**) are considered separately. Catalyst deactivation was assumed to be negligible. Consequently, the concentration of rhodium and ligand were considered to be constant during the reaction. For a batch reaction in a fixed reactor volume the mass balances for the reactants and products are given as Eqs. (9)–(16):

$$\frac{dC_{CO}}{dt} = -r_{hf,1} - r_{hf,2} - r_{hf,3} \qquad (9)$$

$$\frac{dC_{H_2}}{dt} = -r_{hf,1} - r_{hf,2} - r_{hf,3} - r_{hg,1} - r_{hg,2} \qquad (10)$$
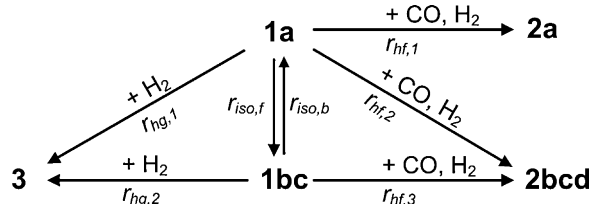
Scheme 2. Reaction network. The rate expressions $r_{hf,1}$, $r_{hf,2}$, $r_{hf,3}$, $r_{iso,f}$, $r_{iso,b}$, $r_{hg,1}$, and $r_{hg,2}$ are incorporated in the mass balances.

$$\frac{dC_{1a}}{dt} = -r_{hf,1} - r_{hf,2} - r_{hg,1} - r_{iso,f} + r_{iso,b} \qquad (11)$$

$$\frac{dC_{1bcd}}{dt} = -r_{hf,3} - r_{hg,2} + r_{iso,f} - r_{iso,b} \qquad (12)$$

$$\frac{dC_{2a}}{dt} = r_{hf,1} \qquad (13)$$

$$\frac{dC_{2bcd}}{dt} = r_{hf,2} + r_{hf,3} \qquad (14)$$

$$\frac{dC_{3}}{dt} = r_{hg,1} + r_{hg,2} \qquad (15)$$

$$\frac{dC_{Rh}}{dt} = \frac{dC_{L1}}{dt} = 0 \qquad (16)$$

For all computations Matlab version 7.7.0.471 (R2008b) was used. Using the built-in function script 'lsqnonlin.m' the so-called objective function was minimized [41]. Vector F is the input for 'lsqnonlin.m' and is defined as follows:

$$F(\bar{p}) = \text{Data} - \text{Model}(\bar{p}) \qquad (17)$$

The objective function is the square of F. 'Data' represents a matrix containing the normalized concentration data obtained at the respective sample times of all the experiments. 'Model' is a matrix, which contains the calculated concentration values for CO to $L1$ of all experiments. The model concentration values were evaluated by solving the mass balances containing the rate equations at the respective experimental sample times. The mass balances were numerically integrated using the built-in ODE solver 'ode113.m'. The rate equations contained the adjustable parameters represented by the vector $\bar{p}$. The optimal values for $\bar{p}$ were calculated using 'lsqnonlin.m'. For the case presented here 'lsqnonlin.m' uses a large scale trust-region reflective Newton method to calculate the optimal set of parameters associated with the minimum value of the square of the function defined in Eq. (17) [41]. To obtain an estimate of the confidence intervals for the optimized values of $\bar{p}$ the built-in Matlab function 'nlparci.m' was used.

3. Results and discussion

3.1. General description of hydroformylation experiments

The reactions were carried out at temperatures ranging from 40 to 80 °C and pressures ranging from 24 to 51 MPa. A temperature of 70 °C was chosen to determine reaction kinetics in detail. At 70 °C the main reaction, the direct formation of **2a** and **2b** from **1a**, CO, and H$_2$ was essentially complete in 1 h with linear over branched aldehyde ratios (*n*:*iso*) ranging between 2.3 and 3.7. Generally, the sum of the concentrations of **1a** and the reaction products determined by sampling from either the top or bottom of the reactor was the same, indicating that the reaction took place under single phase conditions (see Supplementary Information section A.1).

The concentrations of reactants and products as a function of time for a typical hydroformylation experiment conducted in CO$_2$ with **L1** as the ligand are depicted in Fig. 2. The corresponding reaction conditions are given in Fig. 1. The concentrations of CO and H$_2$ after the start of the reaction were derived from the stoichiometry of the reactions and the measured concentrations of the reaction products. After 1 h of reaction the concentration of **2a** was almost constant. The catalyst derived from **L1** gave rise to a significant amount of octene isomers (**1b–g**), resulting in a maximum concentration of 0.034 mol L^{-1} octene isomers after approximately 0.3 h of reaction (Fig. 2b). It can be seen that after almost complete conversion of **1a** the concentration of **2a** remained constant. As a result of the hydroformylation of internal octene isomers (mainly **1b** and **1c**) the concentrations of **2b**, **2c**, and **2d** continuously increased, which is most clearly shown for **2c** and **2d** in Fig. 2b. As a result,
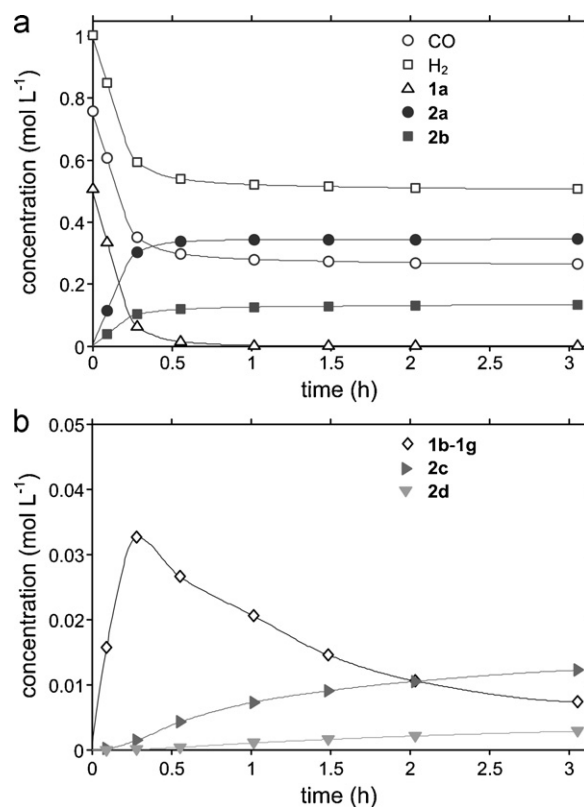
Fig. 2. (a) Concentrations (calculated as explained in Section 2) of the main reactants and products and (b) concentrations of isomers as a function of time for a hydroformylation experiment with ligand **L1**. Experimental conditions: $T = 70$ °C, $C_{Rh} = 2.6 \times 10^{-4}$ mol L^{-1}, $C_{L1} = 1.0 \times 10^{-3}$ mol L^{-1}, $C_{CO_2} = 15$ mol L^{-1}. Note that the initial concentrations of **1a**, CO and H$_2$ at $t = 0$ h are based on the amounts of reactants charged to the reactor and not determined by analysis of a sample. Fig. 1 gives the temperature and pressure as a function of time for this experiment.

the *n*:*iso* ratio decreased slightly at a high conversion of **1a** (reaction time > 0.25 h). Hydrogenation of the product aldehydes into the corresponding alcohols was not observed. Some hydrogenation of **1a** was observed, but isomerization of **1a** was the dominant side reaction.

3.2. Influence of the CO$_2$ amount

Three different amounts of CO$_2$ were applied, namely 1.2, 1.4, and 1.6 mol in a fixed reaction volume of 0.108 L, for the hydroformylation of 55 mmol of **1a**. In Table 1 conditions and results are shown for the corresponding experiments. P_{max} is the pressure reached when the alkene is injected at $t = 0$ h. In the case that 1.2 mol of CO$_2$ was used, a two-phase reaction mixture was observed during the reaction. Significantly higher total concentrations, derived from the sum of the concentrations of **1a** and reaction products, were determined by GC-analysis of samples taken from the bottom part of the reactor [42]. Both the use of 1.4 and 1.6 mol of CO$_2$ resulted in a single phase mixture throughout the course of the reaction.

Using 1.2 mol of CO$_2$ resulted in a significantly higher *n*:*iso* ratio (3.8 after 3 h) and a reaction rate about 10% higher compared to entries 2 and 3. The result obtained using 1.4 mol of CO$_2$ (entry 2, Table 1) is rather similar to the result obtained when 1.6 mol of CO$_2$ was used (entry 3, Table 1). The regioselectivity expressed in *n*:*iso*$_{3h}$ and S$_{2a,3h}$ are about 3.3–3.4 and 77–78%, respectively. The initial reaction rates found when using either 1.4 or 1.6 mol of CO$_2$ are also very similar. The total drop in pressure as result of reaction and sampling (ΔP in Table 1) is of the same order of magnitude

Table 1
Results of the hydroformylation at different pressures.[a]

Entry	n_{CO_2} (mol)	P_{max} (MPa)	ΔP^b (MPa)	$R_{1a,0}$ (10^{-6} mol s^{-1})	$R_{ald,0}$ (10^{-6} mol s^{-1})	TOF_{ald} (10^3 mol$_{ald}$ mol$_{Rh}$ h^{-1})	$S_{2a,3h}$ (%)	$n:iso_0^c$	$n:iso_{3h}$
1[d]	1.2	24.0	7.1	60	56	7.6	78	4.2	3.8
2	1.4	30.5	9.5	54	51	6.5	77	3.8	3.4
3	1.6	40.2	12	54	50	6.6	76	3.6	3.3

[a] General conditions: $V_{reactor}$ = 0.1076 L, stirrer speed = 700 rpm, T = 70 °C, n_{CO} = 108 mmol, n_{H_2} = 108 mmol, n_{1a} = 55 mmol, n_{Rh} = 27 μmol, n_{L1} = 1.35 mmol.
[b] Total change in pressure as a result of reaction and sampling.
[c] The $n:iso$ ratio calculated with the initial rates, see Section 2.
[d] Two-phase system.

as the difference in initial pressure for these experiments. It can thus be concluded that the change in CO_2 concentration as well as the absolute pressure drop has little effect on the kinetics of the reaction when a CO_2 amount in the range of 1.4–1.6 mol is used. Further experiments to study the kinetics were carried out with 1.6 mol of CO_2.

3.3. Description of the reaction rates and selectivity with a kinetic model

At a temperature of 70 °C and with a fixed amount of 1.6 mol of CO_2 the effect of varying the (initial) concentration of a reactant or catalyst precursor was investigated. In Table 2 the conditions and selected results on the initial rate and selectivity of the hydroformylation of **1a** in CO_2 rich mixtures are shown.

Generally, the initial differential $n:iso$ ratio ($n:iso_0$) was higher than the $n:iso$ ratio obtained after 3 h reaction ($n:iso_{3h}$, see Supplementary Information). This was a result of the hydroformylation of internal octenes, mainly 2-octene, at a high **1a** conversion. In the initial stage of the reaction hydroformylation of internal alkenes was not yet significant. It can be seen in Table 2 that in all cases the initial rate of conversion of **1a** ($R_{1a,0}$) was higher than the formation rate of aldehydes ($R_{ald,0}$). Most of the **1a** that was not converted into aldehydes was isomerized to internal octenes ($R_{1b-g,0}$). The **L1** modified Rh catalyst was highly active in hydroformylation with TOF values ranging from 3300 to 9300 mol$_{ald}$ mol$_{Rh}$ h^{-1}.

For each experiment in Table 2 concentrations of reactants and products were determined as a function of time. Consequently, each batch experiment gave considerable information with regard to the reaction kinetics. In order to obtain more insight into the underlying kinetic parameters of the individual reactions, we chose to use a

kinetic model which could fit all the concentration data. The kinetic model can describe the concentrations of reactants and products as a function of time using mass balances derived for a fixed volume batch reactor:

$$\frac{dC_i}{dt} = \sum v_{ij} r_j \tag{18}$$

with C_i being the concentration of reactant or product i, r_j the reaction rate for a certain reaction step j, and v_{ij} the stoichiometry of step j with respect to reactant or product i. Applying this kinetic model we tested several empirical rate equations (r_j) in order to get the best description of the experimental data using the reaction network described in Scheme 2. Using this kinetic model the hydroformylation mechanism can then be discussed in more detail. For each reactant generally three different initial concentration values were chosen. Each experiment described in Table 2 corresponded to about 6–8 data points per reactant or product and this was sufficient to obtain an accurate kinetic model.

For the hydroformylation steps $r_{hf,1}$ and $r_{hf,2}$ (Scheme 2) empirical rate equations of the form closely related to those proposed by Chaudhari and co-workers were used [43,44]. These empirical rate equations for $r_{hf,1}$ and $r_{hf,2}$ show resemblance to the rate equation derived from the catalytic cycle assuming oxidative addition of hydrogen to the acyl-rhodium intermediate as the rate determining step [45]. An increase in the formation rate of **2a** and the small increase in isomerization activity of **1a** (Table 2, $R_{1b-g,0}$) with an increase in ligand concentration was observed. Therefore, a term that describes the weak dependence of the hydroformylation rate (to form **2a**) and the isomerization rate on the ligand concentration was added. Hydroformylation of internal octenes ($r_{hf,3}$) was assumed to be first order in octene and CO. Isomerization ($r_{iso,f}$)

Table 2
Overview of conditions and main results of the experiments.[a] The corresponding concentration profiles were the input for determining the optimal parameter values for the kinetic model and are given in the supporting information.

Entry	p_{max}^b (MPa)	n_{CO} (mmol)	n_{H_2} (mmol)	n_{1a} (mmol)	n_{Rh} (μmol)	n_{L1} (μmol)	$R_{1a,0}^c$	$R_{ald,0}^c$	$R_{2a,0}^c$	$R_{1b-g,0}^c$	TOF_{ald}^d	$n:iso_0$ (−)	$S_{2a,0}^e$ (%)
1[f]	40.6	107	107	55.2	27.3	110	37	34	25	3.0	4.5	2.7	67
2	39.0	81.5	108	54.4	27.7	107	48	44	33	4.1	5.7	2.9	68
3	44.5	162	111	55.0	29.3	110	29	27	19	2.3	3.3	2.3	64
4	38.2	109	86.5	55.0	26.6	107	29	26	19	3.5	3.5	2.6	64
5	44.0	109	166	54.7	26.6	107	79	67	49	11	9.1	2.6	63
6	34.5	109	110	12.1	27.3	107	30	27	19	3.4	3.5	2.5	63
7	52.3	109	110	109	26.6	107	44	40	29	4.1	5.4	2.6	65
8	40.2	108	111	55.4	13.8	55	20	18	12	2.3	4.6	2.4	62
9	39.5	109	109	54.8	52.5	214	93	79	58	14	5.4	2.8	62
10	40.2	109	110	55.1	13.8	104	21	19	13	2.2	4.8	2.6	64
11[f]	40.7	105	108	55.3	27.2	273	46	42	32	3.2	5.6	3.0	70
12[f]	40.2	108	108	54.2	27.2	1359	54	50	39	4.1	6.6	3.6	73
13	49.2	109	108	105	53.2	218	105	99	73	5.9	6.7	2.8	70
14	50.2	108	108	105	53.8	2709	147	132	105	14	8.9	3.7	71
15	50.8	108	108	105	28.1	1344	92	73	56	19	9.3	3.4	61

[a] General conditions: T = 70 °C, $V_{reactor}$ = 0.1076 L, n_{CO_2} = 1.6 mol, stirrer speed = 700 rpm. Note that the amounts can be converted in concentration by dividing with the reactor volume.
[b] Maximum reactor pressure reached upon injection of **1a**.
[c] 10^{-6} mol s^{-1}.
[d] 10^3 mol$_{ald}$ mol$_{Rh}$ h^{-1}.
[e] Initial differential selectivity for **2a**, see Section 2.
[f] Average results of duplicate experiments.

was taken as first order in **1a** and rhodium. For triphenylphosphine and diphosphine modified Rh catalysts a lower CO pressure results in a higher proportion of isomerization and hydrogenation [45,46]. Therefore, a negative order ε in carbon monoxide was taken into account for the isomerization reaction. Hydrogenation rates were assumed to be first order in alkene, hydrogen, and rhodium. The rate equations are given as Eqs. (19)–(24), which together with the mass balances, Eqs. (9)–(16) (see Section 2.5), make up the kinetic model:

$$r_{hf,1} = \frac{k_{hf,1} C_{CO} C_{H_2}^{\beta} C_{1a} C_{Rh}^{\delta}}{(1 + K_{CO,1} C_{CO})^{\alpha} (1 + K_{1a} C_{1a})^{\gamma}} \frac{K_{L1,1} C_{L1}}{(1 + K_{L1,1} C_{L1})} \qquad (19)$$

$$r_{hf,2} = \frac{k_{hf,2} C_{CO} C_{H_2}^{\beta} C_{1a} C_{Rh}^{\delta}}{(1 + K_{CO,2} C_{CO})^{\alpha} (1 + K_{1a} C_{1a})^{\gamma}} \qquad (20)$$

$$r_{hf,3} = k_{hf,3} C_{CO} C_{H_2}^{\beta} C_{1bc} C_{Rh}^{\delta} \qquad (21)$$

$$r_{iso,f} = \frac{k_{iso,f} C_{1a} C_{Rh}}{C_{CO}^{\varepsilon}} \frac{K_{L1,2} C_{L1}}{(1 + K_{L1,2} C_{L1})} \qquad (22)$$

$$r_{hg,1} = k_{hg,1} C_{H_2} C_{1a} C_{Rh} \qquad (23)$$

$$r_{hg,2} = k_{hg,2} C_{H_2} C_{1bc} C_{Rh} \qquad (24)$$

where $k_{hf,1}$, $k_{hf,2}$, $k_{hf,3}$, $k_{iso,f}$, $k_{hg,1}$, and $k_{hg,2}$ are the reaction rate constants for the respective hydroformylation, isomerization, and hydrogenation steps. C indicates the concentration of a reactant or catalyst precursor. α, β, γ, δ, ε, $K_{CO,1}$, $K_{CO,2}$, K_{1a}, $K_{L1,1}$, $K_{L1,2}$ are the empirical kinetic parameters.

At 70 °C the Rh catalyst modified with **L1** resulted in some isomerization of **1a** into internal octenes. The formation of internal octenes is thermodynamically favored relative to **1a**, and the equilibrium concentration of **1a** will be very small [47]. Therefore, we have chosen to neglect the reverse process, i.e. $r_{iso,b} = 0\,mol\,s^{-1}$.

In Table 3 the optimization results and the total residual sum of square errors (RSS) for four different cases are listed. For cases 1 and 2 all data were used as input for the calculation. For cases 3 and 4 the data up to a conversion of 90% were used as input for the calculation. Case 1 is the set of results which were obtained by varying

all 16 parameters to minimize the objective function (Eq. (17), Section 2). When all 16 parameters were included in the optimization the lowest value for RSS was found. In case 2, values for parameters α, β, γ, δ, and ε were used based on the values used in case 1 but rounded off to the closest half integer value. In this case the optimized parameter values differ somewhat from those obtained in case 1. However, the confidence intervals of the optimized values in case 2 have considerable overlap with those of case 1. Also, the RSS value for case 2 is only slightly higher than for case 1. In both cases the values for $k_{hg,1}$ and $k_{hg,2}$ have a small significance, since the corresponding confidence intervals are quite broad.

For case 1 in Table 3 γ has a value of 2, which is the maximum value γ can have according to the optimization routine (Table A7 in Supplementary Information). In the case where $\gamma = 5$ (Supplementary Information section A.5, Table A6, case 6) the confidence intervals for both K_{1a} and γ were rather broad. Therefore, a value for γ higher than 2 was not expected to be meaningful, because it would not result in a significantly enhanced kinetic model.

A model (case 3) where Eqs. (19) and (20) were replaced by versions in which the term describing saturation in **1a** is absent and α is directly associated with the carbon monoxide concentration (Eqs. (25) and (26)) was also tested. This model is similar to the one proposed by Davis and Erkey [38] except for the ligand saturation term that was kept in Eq. (25).

$$r_{hf,1} = \frac{k_{hf,1} C_{CO} C_{H_2}^{\beta} C_{1a}^{\gamma} C_{Rh}^{\delta}}{(1 + K_{CO,1} C_{CO}^{\alpha})} \frac{K_{L1,1} C_{L1}}{(1 + K_{L1,1} C_{L1})} \qquad (25)$$

$$r_{hf,2} = \frac{k_{hf,2} C_{CO} C_{H_2}^{\beta} C_{1a}^{\gamma} C_{Rh}^{\delta}}{(1 + K_{CO,2} C_{CO}^{\alpha})} \qquad (26)$$

The data up to a conversion of 90% (39 samples corresponding to 273 concentration values) were taken into account. Convergence could not be reached when the optimization was tried with all the data (121 samples corresponding to 847 concentration values). Also, the optimization calculations took longer when Eqs. (25) and (26) (on average 6 h) in the optimization were used instead of Eqs. (19) and (20) (on average 0.5 h). Presumably, the computation of

Table 3
Optimization results with 95% confidence intervals.

Parameter[a]	Case 1[b]	Case 2[b]	Case 3[c] (rate equations (25) and (26))	Case 4[c]
$k_{hf,1}$ ($L^{1+\beta+\delta}\,mol^{-1-\beta-\delta}\,s^{-1}$)[d]	754 ± 393	949 ± 166	53 ± 25[g]	1319 ± 310
$k_{hf,2}$ ($L^{1+\beta+\delta}\,mol^{-1-\beta-\delta}\,s^{-1}$)[d]	94 ± 42	111 ± 27	8.7 ± 5.6[h]	95 ± 53
$k_{hf,3}$ ($L^{1+\beta+\delta}\,mol^{-1-\beta-\delta}\,s^{-1}$)[d]	2.17 ± 0.57	2.7 ± 0.5	1.7 ± 2.5[i]	4.7 ± 3.2
$K_{CO,1}$ ($L\,mol^{-1}$)[d]	6.2 ± 2.5	6.04 ± 0.52	31 ± 15[j]	7.1 ± 0.8
$K_{CO,2}$ ($L\,mol^{-1}$)[d]	4.3 ± 1.5	4.03 ± 0.53	19 ± 14[j]	3.9 ± 1.1
K_{1a} ($L\,mol^{-1}$)	0.95 ± 0.68	0.97 ± 0.04	–	0.95 ± 0.04
$K_{L1,1}$ ($10^3\,L\,mol^{-1}$)	2.06 ± 0.13	2.15 ± 0.13	2.22 ± 0.15	2.11 ± 0.13
$K_{L1,2}$ ($10^3\,L\,mol^{-1}$)	4.3 ± 1.9	4.7 ± 2.4	4.6 ± 4.6	2.2 ± 1.1
$\alpha(-)$	2.50 ± 0.19	2.5[f]	2.07 ± 0.07	2.5[f]
$\beta(-)$	1.02 ± 0.05	1[f]	0.91 ± 0.06	1[f]
$\gamma(-)$	2.0 ± 1.0	2[f]	0.45 ± 0.02	2[f]
$\delta(-)$	0.97 ± 0.02	1[f]	0.97 ± 0.02	1[f]
$\varepsilon(-)$	0.88 ± 0.15	1[f]	1[f]	1[f]
$k_{iso,f}$ ($L^{1-\varepsilon}\,mol^{-1+\varepsilon}\,s^{-1}$)	0.34 ± 0.05	0.31 ± 0.02	0.280 ± 0.054	0.37 ± 0.06
$k_{hg,1}$ ($L^2\,mol^{-2}\,s^{-1}$)	0.035 ± 0.022	0.036 ± 0.022	0.017 ± 0.059	0 ± 0.05
$k_{hg,2}$ ($L^2\,mol^{-2}\,s^{-1}$)	0.28 ± 0.11	0.29 ± 0.11	0.6 ± 1.4	1 ± 1
RSS[e] ($mol^2\,L^{-2}$)	0.1446	0.1458	0.1121	0.1010

[a] The parameters $k_{hf,1}$ to $k_{hg,2}$ are part of the vector $\bar{p}$ in the optimization function F.

[b] Calculation using all data up to 100% conversion (121 samples corresponding to 847 concentration values).

[c] Calculation using data up to 90% conversion (39 samples corresponding to 273 concentration values).

[d] The units of $k_{hf,1}$, $k_{hf,2}$, $k_{hf,3}$, $K_{CO,1}$, and $K_{CO,2}$ are dependent on the values of α (for case 3), β, γ (for case 3) and δ.

[e] The residual sum of squares.

[f] These parameters were at a fixed value and were not part of the optimization calculations.

[g] Unit: $L^{1+\beta+\gamma+\delta}\,mol^{-1-\beta-\gamma-\delta}\,s^{-1}$.

[h] Unit: $L^{1+\beta+\gamma+\delta}\,mol^{-1-\beta-\gamma-\delta}\,s^{-1}$.

[i] Unit: $L^{1+\beta+\delta}\,mol^{-1-\beta-\delta}\,s^{-1}$.

[j] Unit: $L^{\alpha}\,mol^{-\alpha}$.
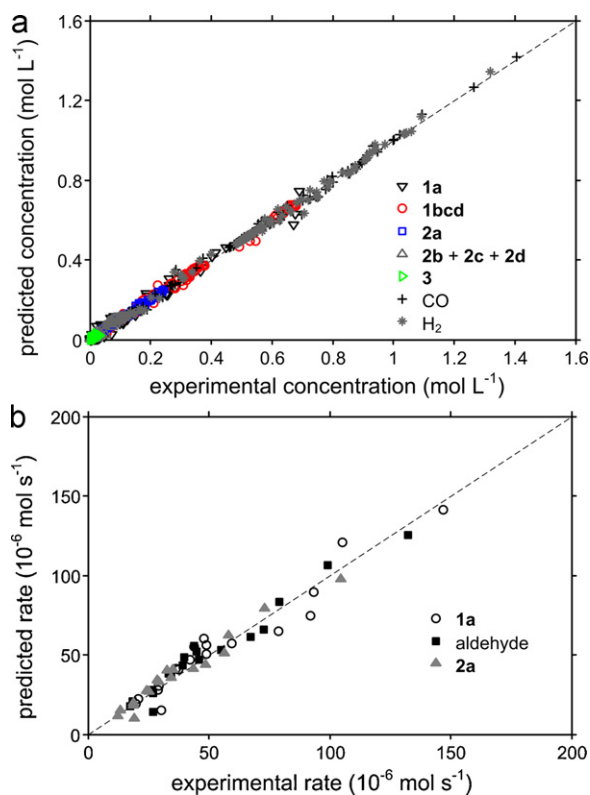
Fig. 3. (a) Comparison of the experimental concentrations and the predicted concentrations obtained with the parameters of case 1 in Table 3. (b) Comparison of the experimental rates and the predicted rates obtained with the parameters of case 1 in Table 3 using the same 'linearized' approach as used for the experimental data.

the differential equations becomes problematic with Eqs. (25) and (26) when the concentrations of **1a** and carbon monoxide approach zero. In Table 3 results are given for this optimization using the rate equations (25) and (26) together with rate equations (21)–(24) (case 3).

The values obtained for α, β, γ, and δ, correspond to some extent to the values reported by Davis and Erkey who have found values of 1.61 ± 0.23 for α, 0.83 ± 0.05 for β, 0.40 ± 0.04 for γ, and 0.94 ± 0.08 for the order in catalyst at a ligand to Rh ratio of 3 to 1 [38]. The optimization was also performed using rate equations (19)–(24) with fixed values for α, β, γ, δ, and ε with the data up to a conversion of 90% (case 4, Table 3). The residual sum of square errors was considerably smaller than obtained with rate equations (25) and (26). Apparently, the kinetic model based on Eqs. (19) and (20) (cases 1, 2 and 4) gives a better description of the data than the kinetic model with the rate equations proposed by Erkey and co-workers (case 3).

In Fig. 3a the calculated concentration data with the optimized parameters of case 1 in Table 3 are compared to the experimental concentration data. Fig. 3a gives no indication of systematic errors and, therefore, it can be concluded that the model gives a good representation of the experimental data. In Fig. 3b a parity plot is used to compare the experimentally determined initial reaction rates ($R_{\mathbf{1a},0}$, $R_{\mathbf{ald},0}$, $R_{\mathbf{2a},0}$ in Table 2) to the initial rates predicted with the model using the same 'linearized' approach as used for the experimental data. The initial rates calculated with the kinetic model agree well with the experimentally determined rates. In the supplementary information further comparisons between experimental and predicted data are provided for cases 3 and 4 in Table 3.

In Fig. 4 concentration-time profiles are given for the experiments in which the initial carbon monoxide concentration has been varied. The lines represent the results obtained with the model. Fig. 4 shows that the prediction based on the kinetic model with the optimized values in Table 3 (case 1) gives a satisfactory description of the concentration data of **1a**, **2a**, branched aldehydes and internal octenes. The model gives a good description of the influence of carbon monoxide on the regioselectivity as well. This can be seen in Fig. 4b and c, because the concentrations of **2a** and **2b**–**2d** as a function of time are represented correctly.

3.4. Influence of temperature and the apparent activation energy

In Fig. 5 the aldehyde yield as a function of time is given for different reaction temperatures using a ligand amount of 0.11 mmol.
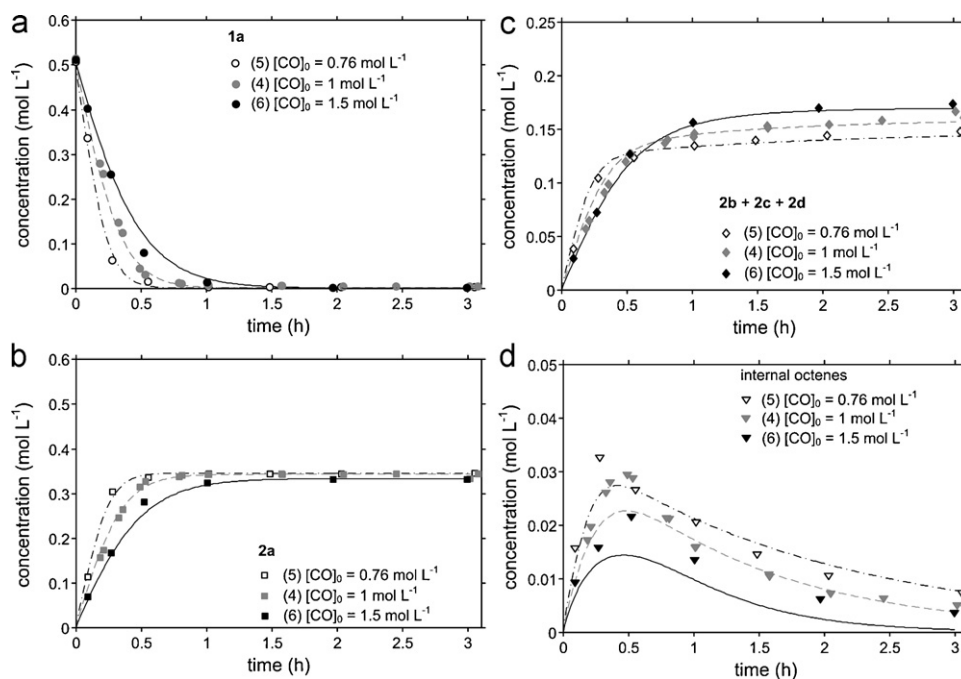
Fig. 4. Comparison of the experimentally obtained normalized concentration profile of **1a** (a), **2a** (b), **2b**–**2d** (c), and **1b**–**1g** (d) indicated by markers and the predicted model concentration profiles indicated by the lines: $[CO]_0 = 0.76$ mol L^{-1} — · — · —, $[CO]_0 = 1$ mol L^{-1} – – –, $[CO]_0 = 1.5$ mol L^{-1} ——.
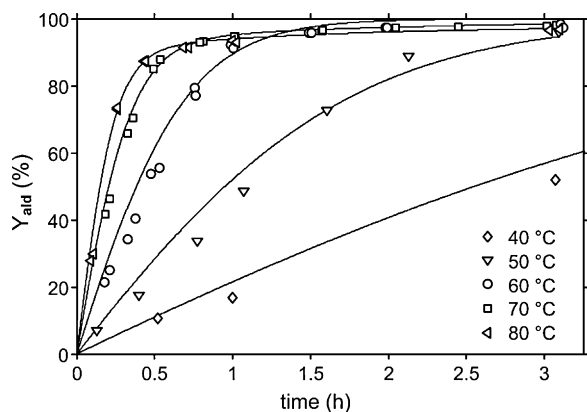
Fig. 5. Comparison of the experimentally determined aldehyde yield (markers) and the aldehyde yield predicted with the kinetic model (lines).

The initial rate of aldehyde formation increased with a factor of 2–2.5 with every 10 °C increase in reaction temperature in the range of 40–70 °C. With a value between 2.7 and 2.9 the $n{:}iso_0$ did not vary significantly with the temperature. However, the initial rate of isomerization $R_{1b–g,0}$, increased with temperature (Table A3 in the supplementary information).

The solid lines in Fig. 5 are predictions based on the kinetic model, calculated with the optimized parameters $k_{hf,1}$, $k_{hf,2}$, $k_{hf,3}$, $k_{iso,f}$, $k_{hg,1}$, and $k_{hg,2}$, and with fixed values for $K_{CO,1}$, $K_{CO,2}$, K_{1a}, $K_{L1,1}$, $K_{L1,2}$ α, β, γ, δ and ε, as given in Table 3 (case 1). In principle, all 16 kinetic parameters presented for case 1 in Table 3 can be temperature dependent. To obtain the best estimate for the temperature dependency of all these parameters, reaction kinetics should be measured at several temperatures. Since we do not have the details of the reaction kinetics at different temperatures, we have assumed that the reaction orders (α, β, γ, δ, and ε) and the parameters $K_{CO,1}$, $K_{CO,2}$, K_{1a}, $K_{L1,1}$, $K_{L1,2}$ are temperature independent. A similar approach was taken by Davis and Erkey [38]. By doing so it is possible to obtain the temperature dependence of $k_{hf,1}$ and $k_{hf,2}$. Subsequently, estimates for the apparent activation energies $E_{act,1}$ and $E_{act,2}$ can be made by means of the Arrhenius equation, Eq. (27):

$$k_{hf,i} = k_{0,i}\, e^{-E_{act,i}/RT}, \quad i = 1 \text{ for } R_{2a,0}, \quad i = 2 \text{ for } R_{2b,0} \qquad (27)$$

with $k_{0,i}$ being the pre-exponential factor, T the temperature, and R the gas constant. In Fig. 6 the natural logarithm of $k_{hf,1}$ and $k_{hf,2}$ are given as a function of $(R \times T)^{-1}$. The data point corresponding to 80 °C was not taken into account to determine the respec-
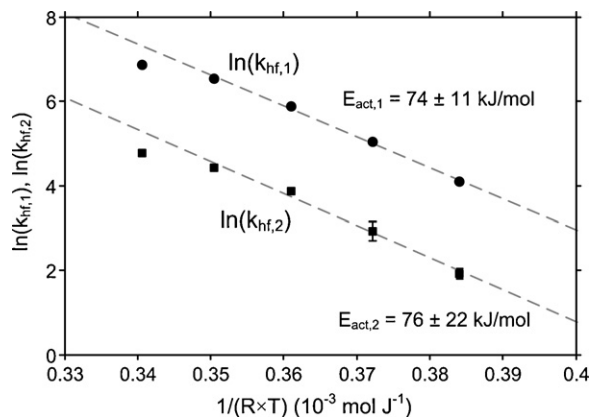
Fig. 6. Apparent activation energy for the formation of the linear (**2a**) and branched aldehydes (**2b**–**2d**). The data point at 80 °C has not been used in the estimation of the apparent activation energy. Every data point has error bars, but in some cases these are not visible as a result of a relatively small error.

tive activation energies. The data point corresponding to 80 °C, at 3.4×10^{-4} mol J^{-1}, appears to deviate from the linear trend when considering the values of $\ln(k_{hf,1})$ and $\ln(k_{hf,2})$ at 40–70 °C. The deviation of this data point is most likely due to the relatively low sampling frequency in combination with the fast reaction, which results in an underestimation of the initial reaction rate. In addition, the initial rate of isomerization to internal octenes is higher at 80 °C than at 70 °C and the formed internal octenes might inhibit the hydroformylation of **1a** (see Supplementary Information, Table A3). The estimated activation energies, with 95% confidence intervals, are 74 ± 11 kJ mol^{-1} for the formation of **2a** and 76 ± 22 kJ mol^{-1} for the formation of **2b**, in the temperature range of 40–70 °C. These values are in the range of values reported Rh-catalyzed hydroformylation of ethene, propene, and **1a** [38,48,49]. The results on $k_{hf,3}$, $k_{iso,f}$, $k_{hg,1}$, and $k_{hg,2}$, in particular, at the low reaction temperatures (≤ 60 °C) could not be determined accurately enough to determine activation energies for the corresponding reaction steps. This is evidently a result of the low isomerization and hydrogenation activity at a temperature below 70 °C. In the Supplementary Information the optimized values for $k_{hf,1}$, $k_{hf,2}$, $k_{hf,3}$, $k_{iso,f}$, $k_{hg,1}$, and $k_{hg,2}$ are given.

3.5. The catalytic cycle and comparison with literature

In Scheme 3 the generally accepted mechanism of hydroformylation is depicted. It is based on the reaction mechanisms suggested by Wilkinson and co-workers for the starting compound HRhCO(PPh$_3$)$_3$ [50], and by Heck based on the starting compound HCo(CO)$_4$ [51]. The so-called dissociative pathway with sequence **C2–C4–C5–C6–C7–C8**, or **C2a–C4a–C5a–C6a–C7a–C8a**, has been generally accepted as the main mechanism for the hydroformylation of alkenes. Starting from **C1** or **C3**, the first step is the dissociation of PR$_3$ or CO, respectively, to form the reactive intermediate **C2**. An alkene coordinates then to **C2** resulting in complex **C4**. Through migratory insertion of the alkene into the Rh–H bond complex **C5** is formed. Subsequently, CO coordinates to **C5**, which results in the n-alkyl **C6**. A second migratory insertion but now of CO into the Rh-alkyl bond then can take place to form **C7** followed by oxidative addition of dihydrogen to form **C8** and reductive elimination to form aldehyde product and the intermediate **C2**. This is still a simplified scheme. For a more detailed discussion the reader is referred to Refs. [3,4,45] and the references cited therein.

Besides the formation of linear aldehydes from the linear 1-alkenes, a certain amount of branched aldehydes is formed. This can be explained by 2,1-insertion of the alkene in **C4** to form the branched alkyl species **C11** [52,53]. **C11** can result in the formation of **2b** through CO insertion, oxidative addition of H$_2$ and reductive elimination of the branched aldehyde product similar to the sequence **C5–C6–C7–C8–C2**. β-Hydrogen elimination from **C11** results in 2-octene that can undergo further isomerization (through reinsertion/β-hydrogen elimination steps) or hydroformylation. In general, the HRhCO(PPh$_3$)$_3$ system has a reasonably high selectivity for the n-aldehyde which can be explained by the high preference for 1,2-insertion of the 1-alkene into the Rh–H bond combined with a low isomerization activity.

A number of empirical models for the reaction rate of the hydroformylation with Rh-catalysts have been proposed. Van Leeuwen and co-workers discussed two types of simplified rate equations (Eqs. (28) and (29)) as a starting point for the modeling of the reaction kinetics [3,54,55]:

$$R_I = \frac{p_1 C_{alkene} C_{Rh}}{p_2 + C_{Ligand}} \qquad (28)$$

$$R_{II} = \frac{p_3 C_{H_2} C_{Rh}}{p_4 + C_{CO}} \qquad (29)$$
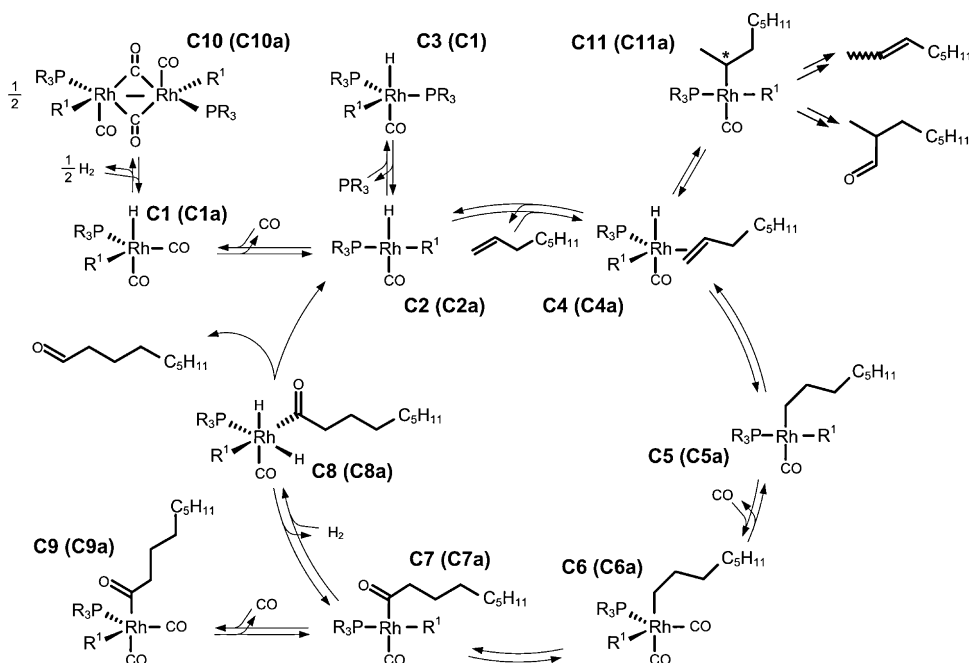
Scheme 3. The catalytic cycles of the hydroformylation of 1-octene, **1a**, to nonanal, **2a**. R_3P is the monodentate phosphine ligand **L1** with $R = -C_6H_3-3,5-(CF_3)_2$. The Rh species with $R^1 = -PR_3$ are designated with the code outside of the brackets. The Rh species with $R^1 = -CO$ are designated with the code inside the brackets.

where p_1 to p_4 are constants. The generally accepted rate equation is R_I (Eq. (28)), for which alkene coordination or the insertion of the alkene into the Rh–H bond can be considered to be the rate-determining step, i.e. the sequence **C2**–**C4**. Type I kinetics (Eq. (28)) is associated with Rh-catalysts modified with triphenylphosphine [48,54]. Type II kinetics (Eq. (29)), which is considered to be less common, has been observed for Rh-catalysts coordinated with CO [56,57] and bulky phosphites, like tris(2-t-butyl-4-methyl-phenyl) phosphite [54,58] but has also been observed for HRh(CO)(PPh_3)_3 [44]. For type II kinetics the rate-determining step is considered to be the oxidative addition of dihydrogen, i.e. the step **C7**–**C8**. Although CO is needed for step **C5**–**C6** it is usually not rate limiting.

In practice the reaction kinetics of hydroformylation are often more complicated than Eqs. (28) and (29) suggest. In several papers a more extensive rate equation that also incorporates the saturation in alkene has been derived for the case where **C7**–**C8** is the rate determining step [44,59]:

$$R = \frac{\nu_1 C_{CO} C_{H_2} C_{alkene} C_{catalyst}}{1 + \nu_2 C_{CO} + \nu_3 C_{CO} C_{alkene} + \nu_4 C_{CO}^2 C_{alkene} + \nu_5 C_{CO}^3 C_{alkene}} \qquad (30)$$

where ν_1 to ν_5 are the constants in which the rate coefficients and equilibrium constants of the reaction steps in the catalytic cycle are lumped together. The empirical rate equation we have found resembles this theoretically derived rate equation. In addition to a first order in dihydrogen, it also includes the saturation kinetics in CO, alkene and ligand. A possible higher order inhibition by CO has been explained by the formation of di- and tricarbonyl species such as **C1**, **C1a**, **C9**, and **C9a** that are all outside of the catalytic cycle. The saturation or even inhibition in alkene at higher alkene concentrations is generally explained by the formation of alkene complexes of rhodium alkyl species that are also outside of the catalytic cycle (not shown in Scheme 3) [60].

To further support the discussion, the reaction orders in carbon monoxide, hydrogen, **1a**, rhodium, and ligand are plotted as a function of their respective normalized concentrations in Fig. 7. When considering the rate equations for $r_{hf,1}$ and $r_{hf,2}$ it is clear that β and δ directly represent the orders in H_2 and Rh, respectively. For CO, **1a**, and **L1** the reaction order cannot be readily discerned from
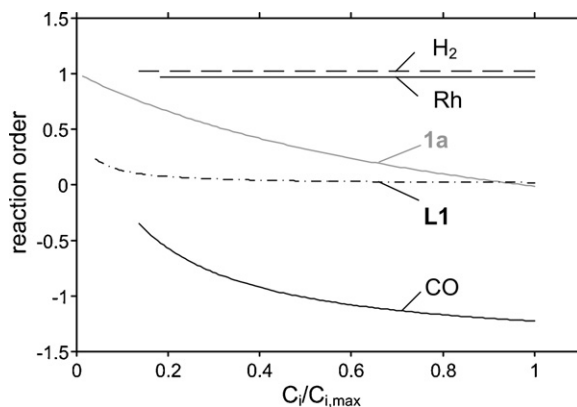
Fig. 7. Reaction order as a function of normalized amount of reactant or catalyst precursor based on the kinetic parameter values of case 1 in Table 3. Reference conditions: $C_{CO} = 1\,mol\,L^{-1}$, $C_{H_2} = 1\,mol\,L^{-1}$, $C_{1a} = 0.5\,mol\,L^{-1}$, $C_{Rh} = 2.5 \times 10^{-4}\,mol\,L^{-1}$, and $C_{L1} = 1 \times 10^{-3}\,mol\,L^{-1}$; maximum amounts: $C_{CO,max} = 1.5\,mol\,L^{-1}$, $C_{H_2,max} = 1.5\,mol\,L^{-1}$, $C_{1a,max} = 1.1\,mol\,L^{-1}$, $C_{Rh,max} = 5.5 \times 10^{-4}\,mol\,L^{-1}$, $C_{L1,max} = 2.5 \times 10^{-2}\,mol\,L^{-1}$.

the rate equations. The reaction orders in CO, **1a**, and **L1** (λ_i), for the primary reactions, the formation of **2a** and **2b** from **1a**, were evaluated using the following equation:

$$\lambda_i = \frac{d\ln(r_{hf,1} + r_{hf,2})}{d\ln C_i} \qquad (31)$$

where C_i is the concentration of component i (CO, H_2, **1a**, Rh, and **L1**). Eq. (31) represents the slope of the curve obtained by plotting the logarithm of the rate ($r_{hf,1} + r_{hf,2}$, Eqs. (19) and (20)) as a function of the logarithm of reactant concentration. This is the differential method to evaluate reaction orders [61]. See Section A.5 in the Supplementary Information for formulas defining λ_{CO}, λ_{1a}, and λ_{L1}.

The reaction order in **1a** changes from 1 to zero and even becomes slightly negative when C_{1a} increases. The order in CO, which initially is close to zero, develops into a strong negative order (ca. −1.25) at higher CO concentrations. The orders in

hydrogen and rhodium are approximately one in the range of concentrations investigated. Saturation kinetics are observed in ligand concentration, going from an order of 0.33 at a ligand concentration of 1×10^{-3} mol L^{-1} to essentially zero at a concentration of 2.5×10^{-2} mol L^{-1}.

All in all, in particular at higher **1a** and CO concentration the kinetics of the Rh/**L1** system show resemblance with the type II kinetics (Eq. (29)). The positive effect of hydrogen concentration could in principle also be caused by the equilibrium between **C1** and **C10** [44,62]. However, this is not likely, because the catalyst is formed in the presence of 1 mol L^{-1} hydrogen and 1 mol L^{-1} carbon monoxide. These concentrations of hydrogen and carbon monoxide are considerably higher than commonly applied in experiments using organic solvents. In earlier spectroscopic studies under lower H$_2$ and CO concentrations than applied here it was already found that HRh(**L1**)$_3$CO is converted predominantly into HRh(**L1**)$_2$CO and that dimeric species such as **C10** and **C10a** are not formed in significant amounts [63]. Also in the case of formation of dimeric Rh species one would not expect a clean first order in hydrogen as is found here. Type II kinetics is mostly associated with the use of a rhodium catalyst modified with electron-withdrawing and sterically hindered ligands like bulky phosphites. It is known that the application of electron-withdrawing ligands decelerates the oxidative addition of hydrogen [3]. **L1** contains six electron-withdrawing trifluoromethyl groups, so, **L1** is considerably less basic and more sterically hindered than triphenylphosphine [64,65]. Therefore, it is plausible for **L1** that oxidative addition of hydrogen is the rate determining step under conditions where the olefin concentration is high.

For a rhodium catalyst modified with triphenylphosphine an increase in concentration of species **C3**, which has three coordinated phosphine ligands, is the main cause of a decrease in reaction rate when the triphenylphosphine concentration is increased [1,3,48]. The observation for **L1** that the reaction rates increase with an increase in ligand concentration, i.e. an increase in **L1**:Rh ratio, is in sharp contrast with what is observed for triphenylphosphine–Rh systems. The origin of the observed saturation kinetics rather than the expected inhibition in **L1** might be that **C3** is not kinetically relevant under the reaction conditions [63]. The latter may be explained by the low basicity of **L1** although steric consequences of the bis-meta substitution, in terms of cone angle for example, may play a role too [64,65]. The absence of **C3** even at high ligand concentration was also reported by Moser et al. for rhodium catalysts modified with para-substituted triarylphosphines [66].

It can be assumed that under the reaction conditions employed in this study a part of the catalysis involves rhodium species with only one **L1** ligand, and that hydroformylation through the 'monophosphine cycle' (**C2a–C4a–C5a–C6a–C7a–C8a**) plays a role. This is implied by the clear enhancement of selectivity with an increase in **L1** concentration. An increase in the **L1** concentration would shift the equilibria to such an extent that the cycle starting with **C2** becomes dominant over the one starting with **C2a**. This explanation is in line with the lower basicity of ligand **L1** compared to PPh$_3$ and with spectroscopic studies recently obtained by Haji and Erkey et al. who observed Rh(acyl)(CO)$_3$(**L1**), a species corresponding to **C9a** [63].

The differential selectivity values based on the initial rate measurement for **2a** lie in between 61% and 73% (Table 2) and are moderate [34]. Nevertheless, the n:iso ratios observed for the Rh/**L1** catalyst are comparable to those for the PPh$_3$-modified rhodium catalyst. The lower differential selectivity for **2a** is clearly due to the higher proportion of internal alkenes formed that are only partially hydroformylated to branched aldehydes [14,34]. The high isomerization activity of the **L1**-modified Rh system is most probably also related to the electron-withdrawing ligand system employed [3] and could be another indication of the involvement of monophos-

phine complexes that lack the steric crowding required for a more selective alkene insertion into the Rh–H bond.

A pronounced change in reaction rate and selectivity was found when the CO$_2$ amount was decreased to 1.2 mol (entry 3, Table 1). A similar observation was made in the hydroformylation of 1-hexene in the presence of a Rh-catalyst by Cole-Hamilton and co-workers when they reached biphasic conditions [33]. It is plausible that the higher reaction rate and regioselectivity observed using 1.2 mol of CO$_2$ were the result of the two-phase reaction conditions. In the two-phase reaction system a higher local Rh and **L1** concentration in the lower **1a**- and product-rich phase can be expected.

Although the unique ligand properties of **L1** seem to be responsible for the effects observed, without comparative studies with other solvents it is not possible to assess the exact solvent effect of carbon dioxide on the hydroformylation kinetics. Earlier studies indicated that results obtained in scCO$_2$ could be compared to those obtained in hexane or toluene but in this case much lower and constant partial pressures (0.5 MPa) of CO and H$_2$ were used [13] resulting in significantly lower concentrations of these reagents (0.065 mol L^{-1} CO and 0.033 mol L^{-1} H$_2$ in hexane [67,68]). The fact that similar TOF values were found in this study as for the hydroformylation in hexane in a previous study [13] may be due to the opposite effects of H$_2$ and CO pressure on the rate of hydroformylation.

4. Conclusion

The high activity of the Rh/**L1** catalytic system for the hydroformylation of 1-octene in scCO$_2$ at 40–70 °C is a result of the unique electronic and steric properties of **L1** which cause diphosphine and very likely also monophosphine Rh species to contribute to the catalysis. The current work shows that, despite of the rather exotic but environmentally advantageous solvent system used (scCO$_2$), the kinetics can still be discussed within the classical framework originally proposed by Wilkinson and co-workers for the system HRh(CO)(PPh$_3$)$_3$ [62].

The kinetic model derived here is complementary and more broadly applicable than previously reported models. The rate of formation of linear and branched aldehydes, inhibition by CO, isomerization, the effect of alkene and ligand were all specifically incorporated in one kinetic model. It could be shown that oxidative addition of hydrogen is the rate limiting step. The observed kinetics and the corresponding mathematical model presented here are expected to be of relevance for other rhodium catalysts modified with electron-withdrawing phosphine ligands.

Appendix A. Supplementary data

Supplementary data associated with this article can be found, in the online version, at doi:10.1016/j.molcata.2011.06.012.

References

[1] M. Beller, B. Cornils, C.D. Frohning, C.W. Kohlpaintner, J. Mol. Catal. A 104 (1995) 17–85.
[2] P.W.N.M. van Leeuwen, Homogeneous Catalysis, Understanding the Art , Kluwer Academic Publishers, Dordrecht, 2004, pp. 125–138.
[3] P.W.N.M. van Leeuwen, Homogeneous Catalysis, Understanding the Art , Kluwer Academic Publishers, Dordrecht, 2004, pp. 139–174.

[4] M. Beller, J. Seayad, A. Tillack, H. Jiao, Angew. Chem. Int. Ed. 43 (2004) 3368–3398.
[5] C.W. Kohlpaintner, R.W. Fischer, B. Cornils, Appl. Catal. A 221 (2001) 219–225.
[6] B. Cornils, in: B. Cornils, W.A. Herrmann, I.T. Horváth, W. Leitner, S. Mecking, H. Olivier-Bourbigou, D. Vogt (Eds.), Multiphase Homogeneous Catalysis, vol. 1, Wiley-VCH, 2005, pp. 27–39;
H. Klein, R. Jackstell, M. Beller, Chem. Commun. 17 (2005) 2283–2285.
[7] (a) S. Bektesevic, A.M. Kleman, A.E. Marteel-Parrish, M.A. Abraham, J. Supercrit. Fluids 38 (2006) 232–241;
(b) P.G. Jessop, J. Supercrit. Fluids 38 (2006) 211–231.
[8] P.G. Jessop, T. Ikariya, R. Noyori, Science 269 (1995) 1065–1069.
[9] S. Kainz, D. Koch, W. Baumann, W. Leitner, Angew. Chem. Int. Ed. Engl. 36 (1997) 1628–1630.
[10] D.R. Palo, C. Erkey, Ind. Eng. Chem. Res. 37 (1998) 4203–4206.
[11] (a) L.J.P. van den Broeke, E.L.V. Goetheer, A.W. Verkerk, E. de Wolf, B.J. Deelman, G. van Koten, J.T.F. Keurentjes, Angew. Chem. Int. Ed. 40 (2001) 4473–4474;
(b) E.L.V. Goetheer, A.W. Verkerk, L.J.P. van den Broeke, E. de Wolf, B.-J. Deelman, G. van Koten, J.T.F. Keurentjes, J. Catal 219 (2003) 126–133.
[12] A.M.B. Osuna, W.P. Chen, E.G. Hope, R.D.W. Kemmitt, D.R. Paige, A.M. Stuart, J.L. Xiao, L.J. Xu, J. Chem. Soc. Dalton Trans. 22 (2000) 4052–4055.
[13] A.C.J. Koeken, M.C.A. van Vliet, L.J.P. van den Broeke, B.J. Deelman, J.T.F. Keurentjes, Adv. Synth. Catal. 348 (2006) 1553–1559.
[14] A.C.J. Koeken, M.C.A. van Vliet, L.J.P. van den Broeke, B.J. Deelman, J.T.F. Keurentjes, Adv. Synth. Catal. 350 (2008) 179–188.
[15] D. Koch, W. Leitner, J. Am. Chem. Soc. 120 (1998) 13398–13404.
[16] D.R. Palo, C. Erkey, Organometallics 19 (2000) 81–86.
[17] K.-D. Wagner, N. Dahmen, E. Dinjus, J. Chem. Eng. Data 45 (2000) 672–677.
[18] Y. Shimoyama, M. Sonoda, K. Miyazaki, H. Higashi, Y. Iwai, Y. Arai, J. Supercrit. Fluids 44 (2008) 266–272.
[19] C.T. Estorach, A. Orejón, A.M. Masdeu-Bultó, Green Chem. 10 (2008) 545–552.
[20] D. Bonafoux, Z.H. Hua, B.H. Wang, I. Ojima, J. Fluorine Chem. 112 (2001) 101–108.
[21] S. Kainz, A. Brinkmann, W. Leitner, A. Pfaltz, J. Am. Chem. Soc. 121 (1999) 6421–6429.
[22] Z.K. Lopez-Castillo, R. Flores, I. Kani, J.P. Fackler, A. Akgerman, Ind. Eng. Chem. Res. 42 (2003) 3893–3899.
[23] G. Franciò, K. Wittmann, W. Leitner, J. Organomet. Chem. 621 (2001) 130–142.
[24] W. Leitner, Nature 405 (2000) 129–130.
[25] Y.L. Hu, W.P. Chen, L.J. Xu, J.L. Xiao, Organometallics 20 (2001) 3206–3208.
[26] C.D. Ablan, D. Sheppard, E.J. Beckman, M.M. Olmstead, P.G. Jessop, Green Chem. 7 (2005) 590–594.
[27] A. Galia, A. Cipollina, G. Filardo, O. Scialdone, M. Ferreira, E. Monflier, J. Supercrit. Fluids 46 (2008) 63–70.
[28] M.F. Sellin, D.J. Cole-Hamilton, J. Chem. Soc. Dalton Trans. 11 (2000) 1681–1683.
[29] J.J.M. de Pater, C.E.P. Maljaars, E. de Wolf, M. Lutz, A.L. Spek, B.-J. Deelman, C.J. Elsevier, G. van Koten, Organometallics 24 (2005) 5299–5310.
[30] J.J.M. de Pater, D.S. Tromp, D.M. Tooke, A.L. Spek, B.-J. Deelman, G. van Koten, C.J. Elsevier, Organometallics 24 (2005) 6411–6419.
[31] J.J.M. de Pater, B.-J. Deelman, C.J. Elsevier, G. van Koten, Adv. Synth. Catal. 348 (2006) 1447–1458, and references cited therein.
[32] I. Bach, D.J. Cole-Hamilton, Chem. Commun. 14 (1998) 1463–1464.
[33] M.F. Sellin, I. Bach, J.M. Webster, F. Montilla, V. Rosa, T. Aviles, M. Poliakoff, D.J. Cole-Hamilton, J. Chem. Soc. Dalton Trans. 24 (2002) 4569–4576.
[34] A.C.J. Koeken, N.E. Benes, L.J.P. van den Broeke, J.T.F. Keurentjes, Adv. Synth. Catal. 351 (2009) 1442–1450.
[35] P.G. Jessop, B. Subramaniam, Chem. Rev. 107 (2007) 2666–2694.
[36] M.J. Muldoon, Dalton Trans. 39 (2010) 337–348.

[37] For example: J.D. Unruh, J.R. Christenson, J. Mol. Catal. 14 (1982) 19–34;
H. Klein, R. Jackstell, K.D. Wiese, C. Borgmann, M. Beller, Angew. Chem. Int. Ed. 40 (2001) 3408–3411.
[38] T. Davis, C. Erkey, Ind. Eng. Chem. Res. 39 (2000) 3671–3678.
[39] A.C.J. Koeken, S.J.M. de Bakker, H.M. Costerus, L.J.P. van den Broeke, B.-J. Deelman, J.T.F. Keurentjes, J. Supercrit. Fluids 46 (2008) 47–56.
[40] K.R. Westerterp, W.P.M. van Swaaij, A.A.C.M. Beenackers, Chemical Reactor Design and Operation , 2nd ed., John Wiley & Sons, Chichester, 1984.
[41] The Matworks website: http://www.mathworks.com (last accessed 17.01.11).
[42] Concentrations which are more than 20% higher than the concentration based on the amount of **1a** injected and the volume of the reactor. See also the Supplementary Information.
[43] R.M. Deshpande, R.V. Chaudhari, Ind. Eng. Chem. Res. 27 (1988) 1996–2002.
[44] S.S. Divekar, R.M. Deshpande, R.V. Chaudhari, Catal. Lett. 21 (1993) 191–200.
[45] C.D. Frohning, C.W. Kohlpaintner, H.-W. Bohnen, in: B. Cornils, W.A. Herrmann (Eds.), Applied Homogeneous Catalysis with Organometallic Compounds, vol. 1, 2nd ed., Wiley-VCH, Weinheim, 2002, pp. 31–103.
[46] R.P.J. Bronger, J.P. Bermon, J. Herwig, P.C.J. Kamer, P.W.N.M. van Leeuwen, Adv. Synth. Catal. 346 (2004) 789–799.
[47] T.C. Morrill, C.A. D'Souza, Organometallics 22 (2003) 1626–1629.
[48] P. Cavalieri d'Oro, L. Raimondi, G. Pagani, G. Montrasi, G. Gregório, A. Andreetta, Chim. Ind. 62 (1980) 572–579.
[49] G. Kiss, E.J. Mozeleski, K.C. Nadler, E. VanDriessche, C. DeRoover, J. Mol. Catal. A 138 (1999) 155–176.
[50] D. Evans, J.A. Osborn, G. Wilkinson, J. Chem. Soc. A: Inorg. Phys. Theor. 12 (1968) 3133–3142.
[51] R.F. Heck, Acc. Chem. Res. 2 (1969) 10–16.
[52] W.A. Herrmann, M. Prinz, in: B. Cornils, W.A. Herrmann (Eds.), Applied Homogeneous Catalysis with Organometallic Compounds, vol. 3, 2nd ed., Wiley-VCH, Weinheim, 2002, pp. 1119–1130.
[53] L.A. Oro, D. Carmona, in: J.G. de Vries, C.J. Elsevier (Eds.), The Handbook of Homogeneous Hydrogenation, Wiley-VCH, Weinheim, 2007, pp. 3–30.
[54] A. van Rooy, J.N.H. de Bruijn, K.F. Roobeek, P.C.J. Kamer, P.W.N.M. van Leeuwen, J. Organomet. Chem. 507 (1996) 69–73.
[55] S.C. van der Slot, P.C.J. Kamer, P.W.N.M. van Leeuwen, J.A. Iggo, B.T. Heaton, Organometallics 20 (2001) 430–441.
[56] G.W. Liu, R. Volken, M. Garland, Organometallics 18 (1999) 3429–3436.
[57] J.H. Feng, M. Garland, Organometallics 18 (1999) 417–427.
[58] A. van Rooy, E.N. Orij, P.C.J. Kamer, P.W.N.M. van Leeuwen, Organometallics 14 (1995) 34–43.
[59] M. Rosales, A. Gonzalez, Y. Guerrero, I. Pacheco, R.A. Sanchez-Delgado, J. Mol. Catal. A 270 (2007) 241–249.
[60] R.M. Deshpande, S.S. Divekar, B.M. Bhanage, R.V. Chaudhari, J. Mol. Catal. 77 (1992) L13–L17.
[61] O. Levenspiel, Chemical Reaction Engineering , 3rd ed., John Wiley & Sons, Chichester, 1999, pp. 38–82.
[62] C.K. Brown, G. Wilkinson, J. Chem. Soc. A: Inorg. Phys. Theor. 17 (1970) 2753–2764.
[63] S. Haji, C. Erkey, Tetrahedron 58 (2002) 3929–3941.
[64] C.A. Tolman, Chem. Rev. 77 (1977) 313–348.
[65] K.K. Banger, A.K. Brisdon, C.J. Herbert, H. Ali Ghaba, I.S. Tidmarsh, J. Fluorine Chem. 130 (2009) 1117–1129.
[66] W.R. Moser, C.J. Papile, D.A. Brannon, R.A. Duwell, S.J. Weininger, J. Mol. Catal. 41 (1987) 271–292.
[67] W. Gao, R.L. Robinson Jr., K.A.M. Gasem, J. Chem. Eng. Data 46 (2001) 609–612.
[68] R. Koelliker, H. Thies, J. Chem. Eng. Data 38 (1993) 437–440.